J Electroceram (2009) 23:80–88
DOI 10.1007/s10832-008-9541-z

Defects and transport in Gd-doped $BaPrO_3$

Anna Magrasó · Reidar Haugsrud · Mercè Segarra · Truls Norby

Received: 15 January 2008 / Accepted: 25 July 2008 / Published online: 14 August 2008

Abstract The electrical conductivity of $BaPr_{1-x}Gd_xO_{3-\delta}$ has been characterized by means of the four-point van der Pauw technique at 200–1100 °C as a function of pO_2 and pH_2O. The contributions from ionic charge carriers were investigated by the EMF of concentration cells and the H^+/D^+ isotope effect on the total conductivity. $BaPr_{1-x}Gd_xO_{3-\delta}$ is predominately a p-type electronic conductor under oxidizing conditions, while ionic conduction is barely measurable. Gd(III) substituted for Pr(IV) is charge compensated mainly by electron holes, with protons and oxygen vacancies contributing significantly but as minority defects only at low temperatures (wet conditions) and at high temperatures, respectively. The conductivity behaviour has been modelled under these assumptions to extract thermodynamic parameters for the defect reactions at play. The practical use of this material is limited by its poor chemical stability.

Keywords $BaPrO_3$ · p-type conductivity · Perovskite · Defect chemistry · Point-defects thermodynamics

A. Magrasó (✉) · M. Segarra
DIOPMA Center, Department of Materials Science and Metallurgical Engineering, University of Barcelona, Martí i Franquès 1, 08028 Barcelona, Spain
e-mail: annamagraso@gmail.com

A. Magrasó · R. Haugsrud · T. Norby
Department of Chemistry, Centre for Materials Science and Nanotechnology (SMN), University of Oslo, FERMiO, Gaustadalleen 21, 0349 Oslo, Norway

1 Introduction

The electrical conductivity of $BaPrO_3$ and derived compounds is less studied than some of the similar Ba-based perovskites, such as $BaCeO_3$ and $BaZrO_3$ [1–3], and literature has been contradictory with respect to the predominating charge carrier under different conditions. For instance, Fukui et al. [4] concluded that $BaPr_{1-x}Gd_xO_{3-\delta}$ (GBP) exhibits proton, oxide ion and electron hole conduction for $x \leq 0.3$. The protonic transport number was estimated to be ~0.2 at 500 °C, using measurement of the water concentration on the air electrode in the cell H_2 + 3% H_2O//GBP//air. Besides, Li et al. [5] reported that $BaPr_{0.7}Gd_{0.3}O_{3-\delta}$ (30GBP) exhibits high protonic conductivity of the order of 5×10^{-3} S/cm at 200 °C. EMF measurements performed under H_2O-saturated O_2 and H_2O-saturated H_2 showed that protons dominate the conductivity at 200 °C with proton transport numbers as high as 0.85. As opposed to the two previous studies, Gorelov et al. [6] concluded that $BaPr_{1-x}Y_xO_{3-\delta}$ is a p-type semiconductor throughout the experimental window of $pO_2 = 2.1\times10^4$–10^{-11} Pa at 373–985 °C, while transport numbers for ions and protons proved to be very small. With increasing yttrium content, the conductivity passes through a maximum for $x=0.1$ (0.26 S cm^{-1} at 800 °C, in air). Furthermore, it was observed that the materials gradually decomposed under reducing conditions.

Recently, Mimuro et al. [7] reported on $BaPr_{1-x}Yb_xO_{3-\delta}$ with essentially the same conductivity results as the Gorelov data [6] for $x=0.1$. In addition to four-point electrical measurements, it was attempted to estimate the proton solubility by FT-IR spectroscopy by replacing H^+ with D^+. The amount of isotope exchange was low, indicating a low proton concentration.

We recently reported that the total conductivity of $BaPr_{0.9}Gd_{0.1}O_{3-\delta}$ (10 GBP), does not exhibit any measurable H^+/D^+ isotope effect changing from O_2 + 2.5% H_2O to O_2 + 2.5% D_2O atmospheres from 700 °C down to 200 °C. This shows that protons do not contribute significantly to the conductivity in this material [8]. However, the fact that the conductivity shows a small but significant decrease on going from dry O_2 (30 ppm H_2O) to wet O_2 (2.5% H_2O) indicates that protons still dissolve from water suppressing the concentration of the major charge carrier (electron holes) somewhat.

$BaPrO_3$-based compounds are chemically unstable, which is an added difficulty for the study of the materials. They readily react with CO_2 to form barium carbonate [5, 9]. Moreover, pure and acceptor-doped $BaPrO_3$ decompose under humid atmospheres to form barium and praseodymium hydroxides if the temperature gets too low, and under reducing conditions by reduction of Pr(IV) to Pr(III) and formation of BaO [6, 9].

In this paper we follow up our previously reported work and clarify further the nature of the electrical conduction in Gd-doped $BaPrO_3$ materials based on a detailed interpretation of the conductivity in terms of point defect thermodynamics.

2 Structure and point defects in $BaPr_{1-x}Gd_xO_{3-\delta}$

Jacobson et al. [10] investigated in the early 1970s structure relations in several perovskites containing tetravalent rare-earth ions. By using room temperature neutron diffraction, $BaPrO_3$ was indexed as orthorhombic *Pbnm* (a=6.181 Å, b=6.214 Å, c=8.722 Å; $c/\sqrt{2}$=6.167). Since the orthorhombic distortion of $BaPrO_3$ with respect the ideal cubic perovskite is small (lattice constants very close to the 1:1:$\sqrt{2}$ ratio), it may be viewed as a quasi-cubic structure.

Li et al. [11] and Mimuro et al. [7] have reported solubility limits of both Gd and Yb of 30–40% in $BaPrO_3$. The first investigation encountered that introduction of the dopant ion first results in a small decrease of the cell volume, followed by an increase up to the solubility limit. This non-monotonic behaviour was interpreted to reflect the variable valence of Pr. Based on later results [9], we have reasons to believe that the practical solubility of Gd in $BaPrO_3$ is substantially lower than 30%.

Substitution of Gd(III) for Pr(IV) introduces effective negative charges that must be compensated by a corresponding amount of effectively positive defects, such as electron holes, oxygen vacancies, or protons. When Gd substitution is charge compensated by oxygen vacancies this can be written according to the Kröger–Vink notation as:

$$2\,BaO + Gd_2O_3 \rightarrow 2\,Ba_{Ba}^{x} + 2\,Gd_{Pr}^{/} + v_o^{\bullet\bullet} + 5\,O_o^{x} \quad (1)$$

Oxygen vacancies, electron holes, and protons are in equilibrium with the surrounding atmosphere according to:

$$O_o^{x} + 2h^{\bullet} = v_o^{\bullet\bullet} + 1/2\,O_2(g) \quad (2)$$

$$H_2O(g) + v_o^{\bullet\bullet} + O_o^{x} = 2\,OH_o^{\bullet} \quad (3)$$

where reaction (3) represents hydration of the oxygen vacancies. The combination of (2) and (3) yields the reaction where instead holes are consumed in the presence of water vapour:

$$1/2\,H_2O(g) + h^{\bullet} + O_o^{x} = OH_o^{\bullet} + 1/4\,O_2(g) \quad (4)$$

Provided that the acceptor, Gd_{Pr}^{I}, is the predominating negative point defect, the electroneutrality condition can be represented by:

$$\left[Gd_{Pr}^{/}\right] = 2\left[v_o^{\bullet\bullet}\right] + \left[OH_o^{\bullet}\right] + \left[h^{\bullet}\right] \quad (5)$$

On basis of the point defect equilibria corresponding to the above reactions, one may assess under which conditions the different defects contribute concentration-wise. The enthalpy of reaction (2) is presumably positive and oxygen vacancies will, consequently, form at high temperatures at the expense of the electron holes—an effect that would be enhanced at lower partial pressures of oxygen. The hydration enthalpy of reaction (3) is usually negative [1, 12, 13] and the proton concentration will, as such, expectedly increase towards lower temperatures at the expense of oxygen vacancies. The enthalpy of reaction (4)—being the sum of a positive and negative enthalpy—is expectedly small and predicts a relatively small temperature dependency of the balance between holes and protons at low temperatures.

3 Experimental

3.1 Preparation and structural characterisation

$BaPr_{1-x}Gd_xO_{3-d}$ (x=0.1 and 0.3) was prepared from $BaCO_3$ (99.95%, Diopma, Barcelona, Spain), Gd_2O_3, and Pr_6O_{11} (both 99.9%, Alfa Aesar, Karlsruhe, Germany) using the acrylamide combustion route described elsewhere [14]. Single-phase perovskites (by XRD, Panalytical X'Pert PRO MPD α1 with Ge (111)-primary monochromator) were obtained after calcination of the combusted gel for 5 h at 1000 °C. The powders were pressed uniaxially at different pressures to obtain specimens with various relative densities for the different types of electrical characterization; ~60 MPa to achieve 80–90% relative densities suitable for fast gas equilibria; and ~120 MPa to reach dense bodies with

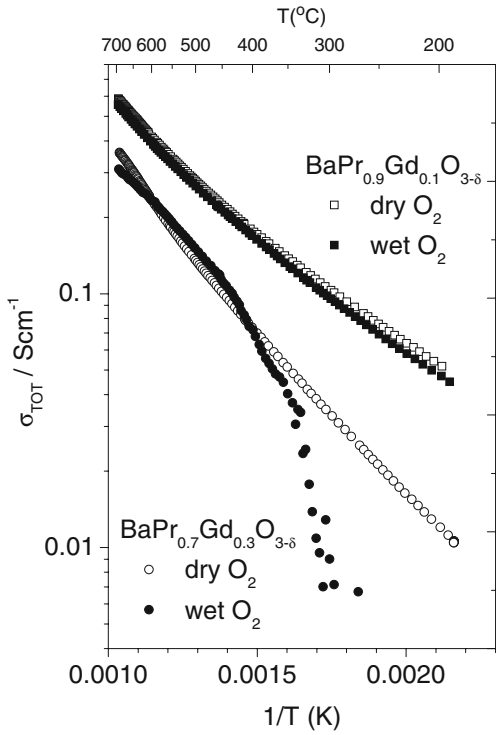

Fig. 1 Comparison of the total conductivity as a function of the inverse temperature between 10% and 30% Gd-doped $BaPrO_3$ under dry and wet O_2 in the temperature range 200–700 °C

relative density >94% for transport number measurements. The sintering was performed at 1400 °C for 5–20 h. (A pellet of the same composition was placed between the alumina and the specimen in order to prevent undesired reactions at high temperature).

The morphology, porosity, and composition of the sintered samples before and after the electrical measurement were characterized by scanning electron microscopy (SEM, Cambridge Instruments Leica Stereoscan 360 or FEI Quanta 200 FEG).

3.2 Conductivity measurements

The electrical conductivity of Gd-doped $BaPrO_3$ was measured in a ProboStat measurement cell (NorECs, Norway) by the four-point van der Pauw method, with Au or Pt wires as electrodes. The conductivities were corrected for porosity using the empirical first approximation $\sigma = \sigma_{\text{measured}}/d_r^2$, where d_r is the relative density.

Conductivity isotherms (from 900 to 200 °C) were measured versus the partial pressure of oxygen in the range 5×10^{-5}–1 atm under dry conditions (~30 ppm H_2O) and, moreover, versus the partial pressure of water vapour in the range ~3×10^{-5} to ~0.025 atm in oxygen. The conductivity was monitored versus time at each new set of conditions to ensure that equilibrium was achieved before taking a measurement. Conductivity isobars were conducted in steps of 25 °C from 1100 to 200 °C in 1, 0.21, and 0.021 atm O_2 under both dry (~30 ppm H_2O) and wet (~2.5% H_2O) conditions. Transport number measurements were attempted on a dense sample (ρ_{rel}=96%) with the setup and procedure described in [15–16].

4 Results

Figure 1 presents the temperature dependence of the total conductivity for samples of $BaPr_{0.9}Gd_{0.1}O_{3-\delta}$ (10 GBP) and $BaPr_{0.7}Gd_{0.3}O_{3-\delta}$ (30 GBP) in the temperature range 200 to 700 °C under dry and wet O_2. Several features for the 30 GBP indicate that it is not stable in the nominal composition: Firstly, in the low-intermediate temperature

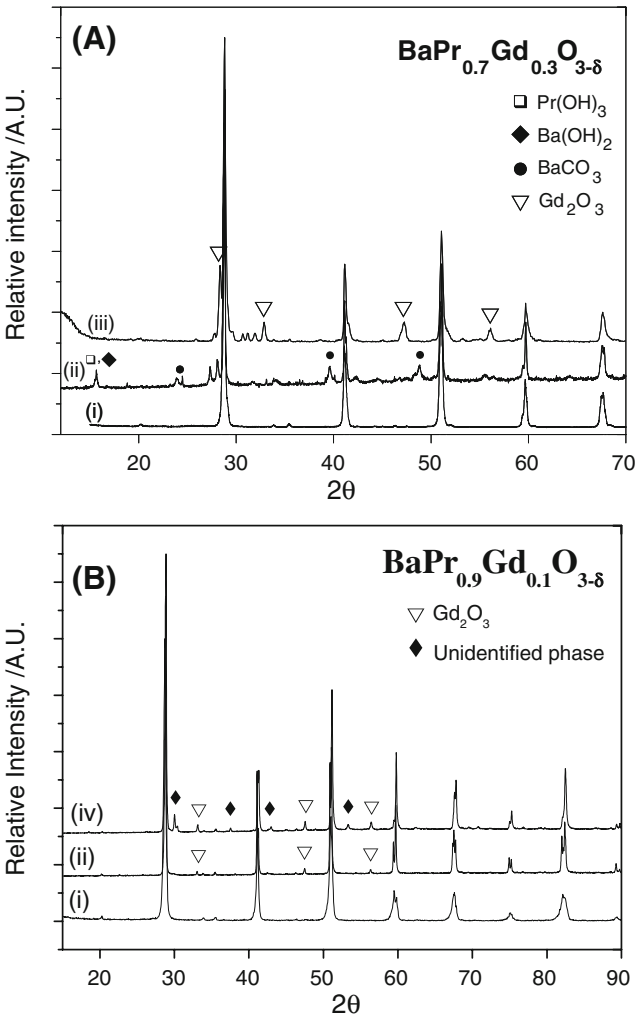

Fig. 2 X-ray diffractograms for (**a**) $BaPr_{1-x}Gd_xO_{3-\delta}$ (x=0.3) and (**b**) x= 0.1, where (*i*) denotes after sintering, (*ii*) after measurement at 700 °C under wet O_2 and either (*iii*) after long thermal treatment at 1500 °C (1–2 days) or (*iv*) after exposure under wet atmospheres at 1100 °C (for some days)

region, the total conductivity is lower than that of 10 GBP, which is the opposite effect of what is expected from the doping level. Under wet oxidising atmospheres, the conductivity exhibits an anomalous decrease upon cooling below ~400 °C, which indicates that the material decomposes. This was verified when the 30GBP was examined by means of XRD after the conductivity measurements [Fig. 2(a), ii]; in addition to the perovskite phase, $Ba(OH)_2$, $BaCO_3$, $Pr(OH)_3$ and Gd_2O_3 were identified. Secondly, microstructural characterization after sintering showed the presence a Gd-rich phase along the grain boundaries [17]. Consequently, 30% Gd clearly is above the solubility resulting in Gd_2O_3 exsolution [Fig. 2(a), iii]. On this basis, no further data is reported on 30 GBP here.

SEM on the 10 GBP specimen after sintering showed that both dense [Fig. 3(a)–(c)] and porous [Fig. 3(d)] bodies were free of secondary phases. After conductivity measurements, SEM and XRD [Fig. 2(b), ii–iii] showed traces of Gd_2O_3, but here no hydroxide formation was detected. Consequently, the stability problems are less critical for 10 GBP than for the 30 GBP specimen. One should, of course, recognize during interpretation of the conductivity data that the solution of 10% Gd is still metastable and that some segregation may occur as a function of time during the measurements. We believe, however, that this would be most pronounced at temperatures above 1000 °C where diffusion rates become sufficient to facilitate segregation. Below this temperature, we consider Gd to be essentially "frozen-in".

Figure 4(a) shows the total conductivity as a function of pO_2 from ~5×10^{-5} (Ar) to 1 atm O_2, every 100 °C from 900 to 200 °C. These experiments were performed under dry conditions to ensure stability. The conductivity is independent of pO_2 at high pO_2, and the pO_2 range increases with decreasing temperature. This corresponds to a limiting electroneutrality condition where $[h^{\bullet}] \approx \left[Gd'_{\mathrm{Pr}}\right] = \text{constant}$. At high temperatures and in the low pO_2-range the conductivity decreases with decreasing pO_2. This corresponds to a change towards a limiting electroneutrality condition where $2\left[v_o^{\bullet\bullet}\right] \approx \left[Gd'_{\mathrm{Pr}}\right] = \text{constant}$, and where electron holes become minority defects concentration-wise.

Effects of the partial pressure of water were investigated, and the results from measurements in oxygen are shown in Fig. 4(b). As evident, the conductivity is essentially independent of the level of water vapour except for a small decrease in the conductivity with increasing amounts of water at low temperatures. To further clarify the significance of this effect, Fig. 5 compares the temperature dependences of the conductivity measured in dry and wet air (pO_2=0.21 atm), and in a dry and wet Ar–air mixture corresponding to pO_2=0.021 atm. The effect of water vapour is more pronounced at lower pO_2. This behaviour can be attributed to protons partly charge compensating the acceptor, with an electroneutrality corresponding to

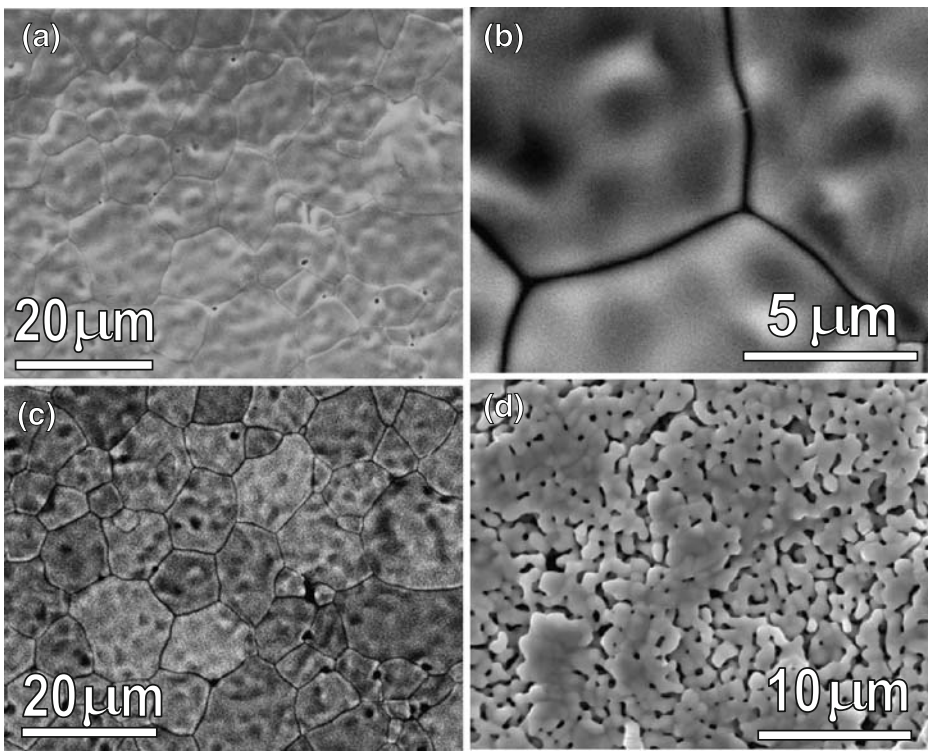

Fig. 3 SEM pictures of $BaPr_{0.9}Gd_{0.1}O_{3-\delta}$ specimens sintered at 1400 °C; a dense sample: (**a**) SE image, (**b**) enlarged selected area (BSE), (**c**) BSE image and (**d**) a porous sample (SE)

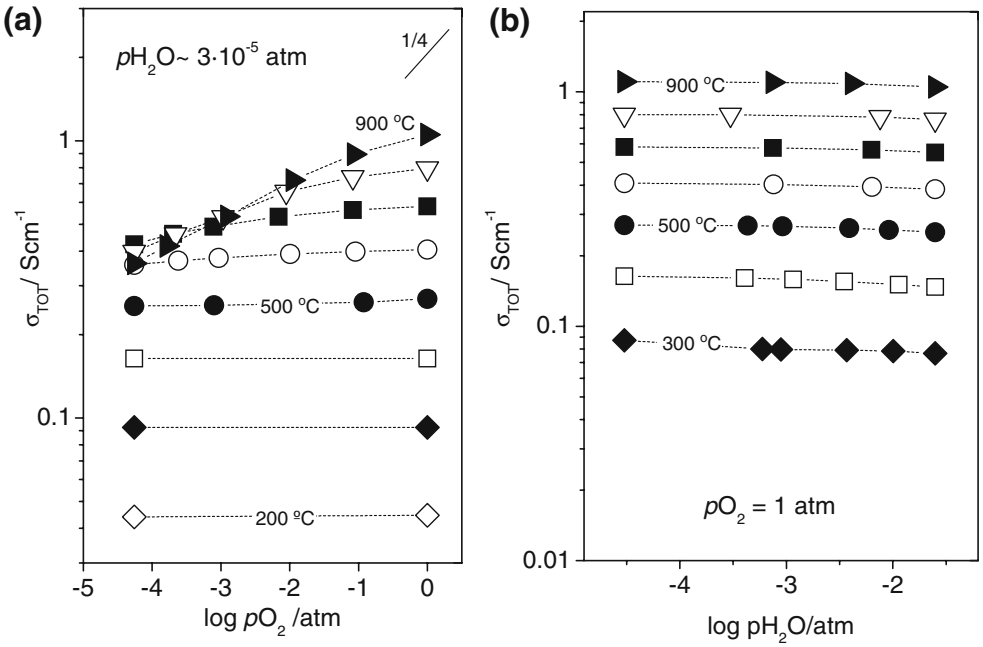

Fig. 4 Total conductivity as a function of the oxygen (dry gases) and water partial pressure (in O_2) for $BaPr_{0.9}Gd_{0.1}O_{3-\delta}$

$\left[Gd'_{Pr}\right] = \left[OH^{\bullet}_{o}\right] + [h^{\bullet}]$ under wet conditions at low temperatures. We should add that the data from Fig. 5 under dry conditions should be pO_2 independent between 5×10^{-5} and 1 atm at temperatures below 600 °C (as demonstrated previously in the pO_2-dependencies, Fig. 4). It is probably a combined exposure to water vapour and subsequent high temperatures, or dopant segregation occurring at high temperatures, that has degraded the sample a little.

From the high temperature data of Fig. 5, one should further note three distinct effects as emphasized by the inset; (I) the bend towards a steeper conductivity curve at around 800 °C, (II) the conductivity levelling off at higher temperatures for the 0.21 and 0.021 atm O_2 isobars and, finally, (III) the increase in the activation energy at temperatures above 1050 °C for the lower pO_2 data. The first bend (I) we attribute to a phase transition towards a higher symmetry structure at higher temperature. In a parallel neutron diffraction (ND) study, temperature induced phase transitions into a cubic phase have indeed been found for undoped and Y-doped $BaPrO_3$ around these temperatures (Knee and Magrasó, in preparation). (ND cannot be done for Gd-containing samples due to a high neutron absorption cross section for Gd). Effects II and III can be rationalized on basis of defect chemistry, as we will discuss in the next sections.

In addition to the van der Pauw measurements, EMF concentration cell measurements (two-electrode setup) were done to try to determine the transport numbers for the ionic partial conductivities. Unfortunately, transport numbers could not be established with confidence below ~900 °C. Above this temperature (and below the melting point of the Au sealing gaskets), gradients in pO_2 across the specimen induced higher EMFs, indicating greater contribution from ionic conduction at those temperatures. Still, the scatter in these voltages was such that no quantitative values for the ionic transport numbers can be reported.

It may be mentioned that AC impedance spectroscopy was early on performed on a two-electrode sample with painted Pt electrodes in the frequency range 1 MHz to 0.1 Hz down to 200 °C. The impedance spectra exhibited a

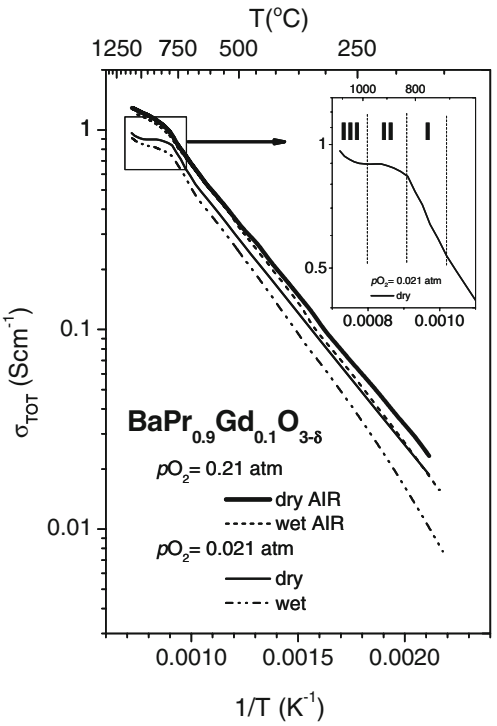

Fig. 5 Total conductivity as a function of the inverse temperature for $BaPr_{0.9}Gd_{0.1}O_{3-\delta}$ at different oxygen partial pressures, both wet and dry, in the temperature range 200–1100 °C

high-frequency semicircle with a capacitance value of ~10^{-8} F, likely to reflect a reaction layer [18]. Such reaction layers have been reported to be formed between the Pt electrode and Y-doped $BaPrO_3$ [6]. The apparent conductivity in this case was more than one order of magnitude lower than corresponding values measured by the four-point van der Pauw set-up. Since the formation of this reaction layer seems unavoidable, we draw the conclusion that two-point measurements are not suitable for characterizing this material.

5 Discussion

In the following, we first discuss the behaviour and modelling of the phase stable below 800 °C. Characterization of the electrical conductivity of $BaPr_{0.9}Gd_{0.1}O_{3-\delta}$ shows that electron holes are the predominant charge carriers in the temperature range 200 to 1100 °C. This may be concluded based on temperature and oxygen pressure dependences, on the small decrease in conductivity with increasing water vapour pressure at low temperature, and moreover, on the low voltages in the EMF measurements and the lack of H^+/D^+ isotope effect on the total conductivity. Although p-type conduction dominates the conductivity through the entire experimental window, the same effects on the conductivity reveal the role of the ionic defects (oxygen vacancies and protons) and allow evaluation of the point-defect relations and thermodynamics. For this purpose we apply standard expressions relating total conductivity, charge carrier concentration and mobility:

$$\sigma_{\mathrm{TOT}} = \sum_i \sigma_i = \sum_i z_i F [i] \delta_M u_i \tag{6}$$

$$u_i = u_{i,0} \frac{1}{T} \exp\left(\frac{-\Delta H_{\mathrm{mob},i}}{RT}\right) \tag{7}$$

Here, z_i, F, $[i]$, δ_M, $u_{i,0}$, $\Delta H_{\mathrm{mob},i}$ are, respectively, the number of charges, Faraday constant, concentration of charge carriers (in mole fraction), molar density (mol/cm^3), pre-exponential of charge mobility and the activation enthalpy of migration of the species i. Since the effects of ionic defects are small (in comparison with electron holes), and chemical stability is an issue, one may expect relatively large uncertainties in the estimated values for Gd:$BaPrO_3$, as will be discussed later on. An important assumption in these equations is that the electron holes behave as small polarons and that p-type conduction, as such, is an activated process. This is not necessarily true in materials with this high electron hole concentration, and a combined trapped/hopping and itinerant model may apply. At intermediate and low temperatures (under dry conditions) where $[h^\bullet] \approx \left[Gd'_{\mathrm{Pr}}\right]$ = constant, the temperature dependence solely reflects the activation enthalpy of hole mobility, and since the value is as high as 30 kJ/mol (0.3 eV) we conclude that the small polaron assumption holds.

In order to model the conductivity data, one has to resolve equations (2)–(5) with respect to the concentration of the different defects given as a function of doping, equilibrium constants, pO_2 and pH_2O under the assumption of equation (5). Since the full model becomes too complex for an analytical solution, we have divided the problem into one solution corresponding to the high temperature defect situation, and one for the low temperature (wet atmosphere) defect situation. The limiting electroneutrality condition and the corresponding expression for the different defects are summarized for the two temperature regimes in Table 1. Note that we express the equilibrium coefficients assuming ideal solution of defects, i.e. we express activities in terms of concentrations. Moreover, since the conductivity contribution from ionic defects is negligible, due to their low mobilities, we have excluded proton and oxygen vacancy partial conductivities from the fitting routine.

To extract values for the thermodynamic parameters of reactions (2) and (4), empirical values for the entropies were used to estimate constraints for the pre-exponential. We write equilibrium constants for reactions 2–4, expressed in terms of the standard enthalpy change of the reaction, ΔH_i^0, as follows:

$$k_i = k_{i,0} \exp\left(\frac{-\Delta H_i^0}{RT}\right) \tag{8}$$

Table 1 Equations used for modelling defect concentrations.

T_{range}	Electroneutrality condition	Equilibrium constant in use	Pre-exponential term of the equilibrium constant	Ionic concentration
Below 500 °C, wet	$\left[Gd'_{\mathrm{Pr}}\right] = [h^\bullet] + \left[OH^\bullet_o\right]$	$k_4 = \frac{\left[OH^\bullet_o\right] p_{O_2}^{1/4}}{\left[O^x_o\right][h^\bullet] p_{H_2O}^{1/2}} = k_{4,0} \exp\left(\frac{-\Delta H_4^0}{RT}\right)$	$k_{4,0} = \frac{\left[\mathrm{OH}^{\bullet 0}_o\right]\left(p^0_{O_2}\right)^{1/4}}{\left[O^{x0}_o\right]\left[\mathrm{h}^{\bullet 0}\right]\left(p^0_{H_2O}\right)^{1/2}} \exp\left(\frac{\Delta S_4^0}{\mathrm{R}}\right)$	$\left[OH^\bullet_o\right] = \frac{\left[O^x_o\right]\left[Gd'_{\mathrm{Pr}}\right] k_4 p_{H_2O}^{1/2}}{\left[O^x_o\right] k_4 p_{H_2O}^{1/2} + p_{O_2}^{1/4}}$
Above 500 °C, dry	$\left[Gd'_{\mathrm{Pr}}\right] = [h^\bullet] + 2\left[v^{\bullet\bullet}_o\right]$	$k_2 = \frac{\left[v^{\bullet\bullet}_o\right] p_{O_2}^{1/2}}{\left([h^\bullet]\right)^2 \left[O^x_o\right]} = k_{2,0} \exp\left(\frac{-\Delta H_2^0}{RT}\right)$	$k_{2,0} = \frac{\left[v^{\bullet\bullet 0}_o\right]\left(p^0_{O_2}\right)^{1/2}}{\left([h^{\bullet 0}]\right)^2 \left[O^{x0}_o\right]} \exp\left(\frac{\Delta S_2^0}{R}\right)$	$\left[v^{\bullet\bullet}_o\right] = \frac{4\left[Gd'_{\mathrm{Pr}}\right] k + \frac{p_{O_2}^{1/2}}{\left[O^x_o\right]} - \sqrt{\frac{8\left[Gd'_{\mathrm{Pr}}\right] k p_{O_2}^{1/2}}{\left[O^x_o\right]} + \frac{p_{O_2}}{\left[O^x_o\right]^2}}}{8k_2}$

Concentration is expressed in mole fraction of species. $\left[O^x_o\right]$ constant (=3) and ideal solid solutions are assumed. The concentration of the ionic species at standard state is considered to be $\left[O^{x0}_o\right]$.

where R and T are the gas constant and the absolute temperature, respectively, and $k_{i,0}$ is a pre-exponential term that involves all the parameters that are ideally independent of temperature, specifically the concentration of species/gases at standard state, and the standard change in entropy, ΔS_i^0. In order to extract ΔS_i^0 from the pre-exponential term, one has to define the standard state of the species involved in the reaction. For gases, the standard state is 1 bar, and for ionic defects (in our case oxygen vacancies, protons, and lattice oxygen) the standard state is defined as full occupancy of the relevant sublattice (in our case the oxygen sublattice). However, in the cases where electrons are involved in the reaction, this is not straightforward since the standard state of electrons is not easily defined. In a small polaron model, however, as in our case, the concentration of sites for electron holes in the standard state may be estimated by assuming that two holes (by degeneracy) can occupy each B–O valence band bond. (Other alternatives may assume there is no degeneracy, or that a hole resides on the B-site and occupies a whole BO_6 octahedron so that a second hole is excluded there. The difference in obtained entropy is below the experimental error in this work). A summary of the expressions used is displayed in Table 1.

Furthermore, the equilibria corresponding to reactions (2), (3), and (4) are not independent, and their equilibrium constants are related as $k_2 \cdot k_3 = k_4^2$, so that the standard enthalpy and entropy change of reaction 4 can be expressed as:

$$\Delta H_4^0 = \frac{\Delta H_2^0 + \Delta H_3^0}{2} \tag{9}$$

$$\Delta S_4^0 = \frac{\Delta S_2^0 + \Delta S_3^0}{2} \tag{10}$$

From previous studies and reviews [1, 12, 13], the standard hydration entropy (ΔS_3^0, for Eq. 3) is typically reported in the range −120±40 J/molK, which corresponds to the empirical value of −120 J/molK for the loss of one gas molecule for chemical reactions in general. Similarly, one could expect that the entropy changes of reaction 2 and 4 correspond to +60 J/molK (formation of 0.5 mol of gas) and −30 J/molK (loss of 0.25 mol of gas), respectively.

Consequently, the standard entropy change for reaction (2) was fixed at +60 J/molK, and the standard enthalpy change, ΔH_2^0, was then fitted to the measured conductivities to be approximately 130 kJ/mol, i.e. positive, as expected. The standard enthalpy change associated with dissolution of protons and consumption of holes in the low temperature region according to reaction (4), ΔS_4^0, was found to be −6 kJ/mol, with the standard entropy change ΔS_4^0 at −37 J/molK. The physical meaning and consequence of these parameters (especially the small negative value of the enthalpy change) is that the material contains few protons under oxidizing conditions, and that their concentration does not increase much with decreasing temperature. Finally, by using the values obtained for ΔH_2^0 and ΔH_4^0 the standard enthalpy change for hydration of oxygen vacancies, ΔH_3^0, was calculated according to (9) to be approximately −140 kJ/mol. The different thermodynamic parameters and mobility parameters for the electron holes with corresponding uncertainty estimates are summarised in Table 2. It is interesting to note that the hydration enthalpy estimated here follows the correlation between hydration enthalpy and difference between the Allred–Rochow electronegativities of the B- and A-site cation occupants (ΔX_{B-A}) as suggested by Norby et al. [13].

In evaluating these thermodynamic parameters, one should recognize the large uncertainties. One reason is that the predominance of electron holes leaves only relatively small effects on the conductivity from the ionic defects. Moreover, since the experimental window where $BaPrO_3$ is sufficiently stable is narrow, electroneutrality conditions where ionic defects fully dominate charge compensation of the acceptor are never reached. Despite this, we believe that these thermodynamic parameters can, to a reasonable degree, represent the point-defect structure of Gd-doped $BaPrO_3$. The concentrations of electron holes, oxygen vacancies and protons are summarized as a function of the inverse absolute temperature under wet and dry conditions in Fig. 6(a) and (b), respectively. Note that proton and oxygen vacancy concentrations increase in the low temper-

Table 2 Fitted parameters of reactions (2, 4) and electron hole mobility for $BaPr_{0.9}Gd_{0.1}O_{3-\delta}$.

	Literature values [15]	*Value*[a], *this work*	*Uncertainty range*[b]
$k_{2,0}/bar^{1/2}$		10^5	10^4–10^5
$\Delta S_2^0/J\,K^{-1}\,mol^{-1}$		60[a]	10–70[b]
$\Delta H_2^0/kJ\ mol^{-1}$		130	100–160
$\Delta S_3^0/J\,K^{-1}\,mol^{-1}$	-120	-134	−(130–210)
$\Delta H_3^0/kJ\ mol^{-1}$	-138	-142	−(110–190)
$k_{4,0}/bar^{-1/4}$		0.1	0.01–0.1
$\Delta S_4^0/J\,K^{-1}\,mol^{-1}$		-37[a]	−(35–70)[b]
$\Delta H_4^0/kJ\ mol^{-1}$		-6	−(5–15)
$\mu_{h,0}/cm^2\ K\ V^{-1}\ s^{-1}$		150	100–200
$\Delta H_{m,h}/kJ\ mol^{-1}$		30	27–33

Hydration entropy and enthalpy (3) have been calculated using Eq. 9 and 10.

[a] Values constrained or a direct result of constraints in the fitting. For clarification on the extraction of the entropy values, see also text.

[b] Ranges resulting from releasing constraint.

ature (wet conditions) and high temperature regions, respectively. The temperature where proton concentration or oxygen vacancy concentration equals that of holes increases, or decreases, respectively, with decreasing pO_2. Thus, the material would have dominant ionic conductivity under more reducing conditions if the material would remain stable.

The data for 10 GBP (in dry O_2 conditions) from Fig. 1 does not follow a simple Arrhenius-type dependence below ~400 °C. The curvilinear shape of the dependence was also reported by Gorelov et al. [6] for $BaPr_{0.9}Y_{0.1}O_{3-\delta}$ in air, but was not commented further. It has been suggested that progressive delocalization of the p-type charge carriers occurs in the p-type electronic conductors with varying pO_2, e.g. for $Pr_{0.5}Sr_{0.5}FeO_{3-\delta}$ on increasing oxygen chemical potential [19], or that the mobility of holes is strongly correlated to the oxygen off-stoichiometry, e.g. for $La_{1-x}Sr_xFeO_{3-\delta}$ [20]. That might give a possible explanation on the differences in the low temperature curves between isobars in dry air (straight) and dry O_2 (curved). It is difficult to ascertain the origin of such an effect in our material, but one may speculate that, since there is a big concentration of holes dominating the defect picture in the material, especially at low temperatures, part of the electron holes may act as itinerant rather than hopping charge carriers, giving rise to a gradual increase of mobility over that expected from the small polaron model.

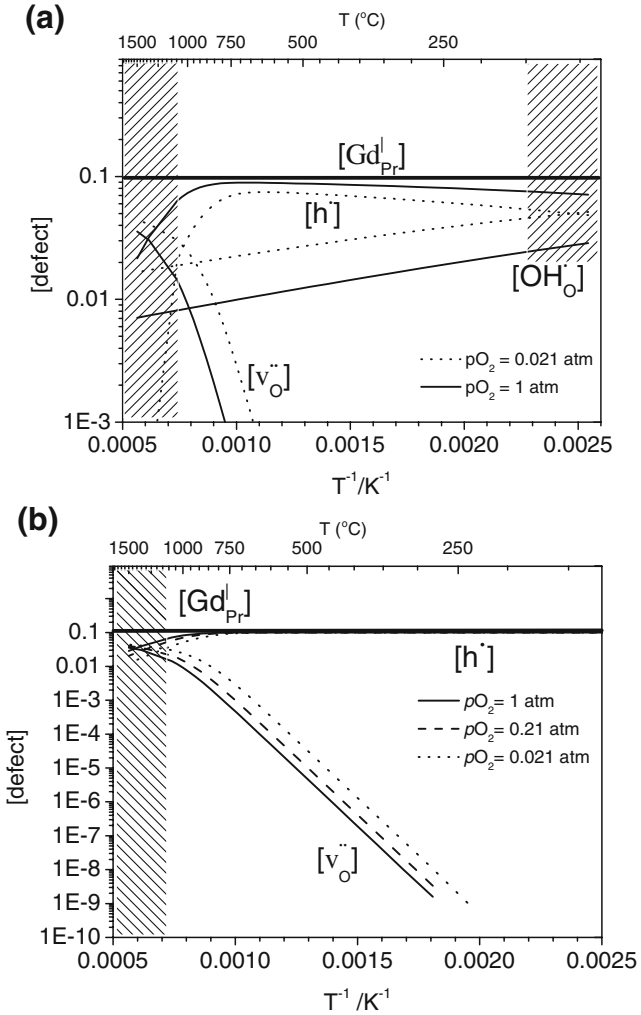

Fig. 6 Proton, oxygen vacancy and electron hole concentration as a function of temperature based on the thermodynamic parameters in Table 2 under wet conditions (**a**) and dry conditions (**b**), where protons are negligible and are not taken into account. The shaded regions denote temperature regions outside the investigated window. Electrons omitted for clarity

With the present data set it has not been possible to report on ionic conductivities. There is a contribution of such defects concentration-wise, but their mobilities are much lower than that of holes. As we have already concluded in a previous paper, proton conductivity does not contribute significantly in Gd-doped $BaPrO_3$ as isotope effects are missing [8].

About the high temperature phase and the conductivity at the uppermost temperatures, the following may rationalise the behaviour: The bend upwards (effect I) may be due to a higher mobility of electron holes as the structure goes more symmetrical. If reaction (2) is shifted more to the right for this phase, we loose holes, and this may explain why the conductivity levels off (effect II). Finally, this leads to an increase of the concentration of oxygen vacancies and a higher activation energy (effect III), especially prominent in the data measured at 0.021 atm O_2, may show an oxide ion conductivity contribution. An equally likely possibility involves the onset of intrinsic electronic conductivity from electrons and holes thermally ionised over the bandgap of the praseodymate.

When it comes to a possible exploitation of $BaPrO_3$-based compounds in e.g. SOFCs, the decomposition of these materials to hydroxides and carbonates in water vapour at moderate and low temperatures and in hydrocarbon derivatives like CO_2 would be detrimental. Moreover, reduction of Pr(IV) to Pr(III) would limit the use of these materials to high oxygen partial pressures, especially at high temperatures.

6 Summary

Gd-substituted $BaPrO_3$ is predominantly a p-type semiconductor under oxidising conditions. Relative to the p-type conductivity, the material does not exhibit any significant ionic conductivity, neither from oxide ions nor protons.

The conductivity data can be interpreted by assuming that the Gd acceptor is charge compensated by electron holes, oxygen vacancies, and protons. Electron holes predominate the electroneutrality condition throughout the entire temperature range, but protons and oxygen vacancies

contribute concentration-wise under wet conditions at low temperatures and at high temperatures, respectively, with increasing effects at low oxygen pressures. Holes migrate according to a small polaron model with an activation energy of 30 kJ/mol (0.3 eV).

Thermodynamic parameters reflecting the variations in the defect concentrations have been estimated for $BaPr_{0.9}Gd_{0.1}O_{3-\delta}$ by modelling of conductivity isobars and isotherms under the given electroneutrality assumption. The corresponding standard enthalpy changes of the reactions were fitted to be $\Delta H_2^0 = 130\,\mathrm{kJ/mol}$ for the reduction of two holes to form one oxygen vacancy, $\Delta H_4^0 = -6\,\mathrm{kJ/mol}$ for the reductive hydration of one hole, and $\Delta H_3^0 = -140\,\mathrm{kJ/mol}$ for the hydration of an oxygen vacancy. The numbers reflect that oxygen vacancies form at the expense of protons and holes at high temperatures, and that the proton concentration remains minor and fairly constant under the dominance of holes, even at relatively low temperatures (400–200 °C). The enthalpy of hydration of oxygen vacancies is exothermic as expected according to a correlation for perovskites, but the dominance of holes suppresses the hydration of the vacancies.

$BaPr_{0.7}Gd_{0.3}O_{3-\delta}$ is an unstable composition, particularly vulnerable under wet conditions undergoing decomposition. $BaPr_{0.9}Gd_{0.1}O_{3-\delta}$ is sufficiently stable for the purpose of this investigation, but one should recognize that a gradual change in the conductivity during long-term exposure and post-measurement characterization of the composition indicates that also 10 mol-% Gd is above the solubility limit in the $BaPrO_3$ perovskite phase under practical operating conditions.

Acknowledgements The authors wish to acknowledge Dr. Albert Tarancón (EME, University of Barcelona) for assistance to obtain part of the experimental data. This work has been supported through the BRD scholarship (University of Barcelona) and CeRMAE centre (Generalitat de Catalunya) for AM and by the Research Council of Norway, grant no. 15851/431 (Functional Oxides for Energy Technology, NANOMAT) for RH.

References

1. K.D. Kreuer, Annu. Rev. Res. **33**, 333–359 (2003) doi:10.1146/annurev.matsci.33.022802.091825
2. H. Iwahara, Solid State Ion. **28–30**, 573 (1988) doi:10.1016/S0167-2738(88)80104-8
3. J. Guan, S.E. Dorris, U. Balachandran, M. Liu, J. Electrochem. Soc. **145**, 1780 (1998) doi:10.1149/1.1838557
4. T. Fukui, S. Ohara, S. Kawatsu, J. Power Sources **71**, 164–168 (1998) doi:10.1016/S0378-7753(97)02813-9
5. L. Li, J.R. Wu, S.M. Haile, Electrochem. Soc. Proc. **12**, 214–223 (2001)
6. V.P. Gorelov, B.L. Kuzin, V.B. Balakireva, N.V. Sharova, G.K. Vdovin, S.M. Beresnev et al., Russ. J. Electrochem. **37**(5), 505–511 (2001) doi:10.1023/A:1016628205030
7. S. Mimuro, S. Shibako, Y. Oyama, K. Kobayashi, T. Higuchi, S. Shin et al., Solid State Ion. **178**, 641–647 (2007) doi:10.1016/j.ssi.2007.02.006
8. K.A. Furøy, R. Haugsrud, M. Hänsel, A. Magrasó, T. Norby, Solid State Ion **178**, 461–467 (2007) doi:10.1016/j.ssi.2007.02.014
9. A. Magrasó, F. Espiell, M. Segarra, J.T.S. Irvine, J. Power Sources **169**, 53–58 (2007) doi:10.1016/j.jpowsour.2007.01.041
10. A.J. Jacobson, B.C. Tofield, B.E.F. Fender, Acta Crystallogr. B **28**, 956 (1972) doi:10.1107/S0567740872003462
11. L. Li, J.R. Wu, M. Knight, S.M. Haile, Electrochem. Soc. Proc. **28**, 58–66 (2001)
12. T. Norby, Y. Larring, Curr. Opin. Solid State Mater. Sci. **2**(5), 593–599 (1997) doi:10.1016/S1359-0286(97)80051-4
13. T. Norby, M. Widerøe, R. Glöckner, Y. Larring, Dalton Trans **19**, 3012–3018 (2004) doi:10.1039/b403011g
14. A. Magrasó, A. Calleja, X.G. Capdevila, F. Espiell, Solid State Ion. **166**(3–4), 359–364 (2004) doi:10.1016/j.ssi.2003.11.019
15. T. Norby, Solid State Ion. **28–30**, 1586 (1988) doi:10.1016/0167-2738(88)90424-9
16. T. Norby, P. Kofstad, J. Am. Ceram. Soc. **67**, 786 (1984) doi:10.1111/j.1151-2916.1984.tb19701.x
17. A. Magrasó, Synthesis and characterization of $BaPrO_3$-based materials for SOFC applications. Doctoral thesis, Faculty of Chemistry, University of Barcelona, Spain, pp. 111–144, 2007
18. J.T.S. Irvine, D.C. Sinclair, A.R. West, Adv. Mater. **2**(3), 132 (1990) doi:10.1002/adma.19900020304
19. V.V. Kharton, M.V. Patrakeev, J.C. Waerenborgh, A.V. Kovalevsky, Y.V. Pivak, P. Gaczynski, A.A. Markov, A.A. Yaremchenko, J. Phys. Chem. Solids **68**, 355–366 (2007)
20. M.V. Patrakeev, I.A. Leonidov, V.L. Kozhevnikov, K.R. Poeppelmeier, J. Solid State Chem. **178**, 921–927 (2005) doi:10.1016/j.jssc.2004.10.038